Annals of Biomedical Engineering, Vol. 28, pp. 1318–1325, 2000
Printed in the USA.

0090-6964/2000/28(11)/1318/8/$15.00

Delayed Activation and Retrograde Propagation in Cardiac Muscle: Implication of Virtual Electrode Effects

JIASHIN WU,[1,3] DAN M. RODEN,[2] and JOHN P. WIKSWO, JR.[1]

[1]Department of Physics & Astronomy, [2]Department of Pharmacology, Vanderbilt University, Nashville, TN and [3]Krannert Institute of Cardiology, Indiana University School of Medicine, Indianapolis, IN

(Received 8 April 1999; accepted 12 September 2000)

Abstract—Point cathodal stimulation of cardiac tissue was shown previously to produce both a dog-bone shaped virtual cathode transverse to the muscle fibers and two longitudinal virtual anodes. We hypothesize that virtual anodes can cause a region of delayed activation, separating two regions of early activation caused by the virtual cathode. Using a high-density electrode array in 42 superfused epicardial slices from 14 canine left ventricles, we observed regions of early and delayed activation and different pathways of retrograde propagation corresponding to the earlier patterns. Retrograde propagation was seen from the transversely located early activation area through areas of delayed activation toward the cathode, and from the early activation area toward the cathode directly. These pathways caused a wide dispersion in the direction of retrograde propagation ($2° \pm 31°$, $n = 179$, relative to the fast axis of threshold activation; radial velocity: 0.5 ± 0.2 m/s, $n = 95$, in 12 slices from 8 hearts with stimuli of 330 μs, 0.8–30 mA). Delayed activations were observed $0° \pm 6°$ ($n = 32$) from the axis in 23 maps (at differing stimulation strengths) recorded in 13 slices from 10 hearts. We conclude that point cathodal stimulation induce delayed activation along the fiber axis and retrograde propagation both along and transverse to the axis. © *2000 Biomedical Engineering Society.*
[S0090-6964(00)00111-9]

Keywords—Heart, Electrophysiology, Bidomain, Reentry.

INTRODUCTION

The induction of fibrillation by a strong stimulus is governed in part by the cable-like properties of the cardiac syncytium. However, the underlying mechanisms are incompletely understood. It was shown in anisotropic bidomain simulation models that adjacent regions of depolarized and hyperpolarized transmembrane potential could be induced with a point current injection.[12,13,15] Simulations predicted that a strong cathodal stimulus can produce a dog-bone shaped region of early activation (the virtual cathode) oriented transverse to muscle fibers, as well as two hyperpolarized regions (the virtual anodes) a few millimeters away from the site of stimulation along the fiber axis. The size and the shape of the virtual electrodes depend upon both membrane and tissue conductivity. These predictions were indeed observed *in vivo*[20] and *in vitro*.[8–10,19] The virtual electrode effects can lead to unidirectional block of conduction. After a strong cathodal stimulus, the transient hyperpolarization at the virtual anodes can block outward propagation from the site of stimulation, while the wave front propagated from the virtual cathode(s) can activate the same regions when arrived later. The unidirectional block of conduction provided the possibility of reentry, which was further enhanced when the stimulus was delivered during the vulnerable period of a prior activation.[14]

The resistivity of cardiac muscle spans a wide range depending on the microanatomy. When tissue resistivity differs from the values used in the simulations and when a bath is present, the shape and the relative locations of the virtual electrodes and the resulted pattern of the propagation of activation can differ from the simulation predictions. With a strong point cathodal stimulation of a tissue slice in a bath, we expected that in addition to the case of forming a dog-bone shaped region of early activation in direct correspondence to the virtual cathode as demonstrated previously,[19,20] there could be another case in which a region of delayed activation along the fiber axis could separate two regions of early activation, when there is sufficient separation between the two enlarged ends of the virtual cathode. In this case, early activations at the regions corresponding to the enlarged ends of a virtual cathode could propagate directly to the site of stimulation at right angles to the fiber orientation, in contrast to the case of a dog-bone shaped region of early activation where retrograde propagation went through the virtual anodes, as described earlier. This study was carried out to explore the range of the patterns of activation and the directions of retrograde propagation.

Address correspondence to Jiashin Wu, PhD, Krannert Institute of Cardiology, Dept. of Medicine, Indiana University School of Medicine, 1111 West 10th Street, Indianapolis, IN 46202. Electronic mail: jiaswu@iupui.edu

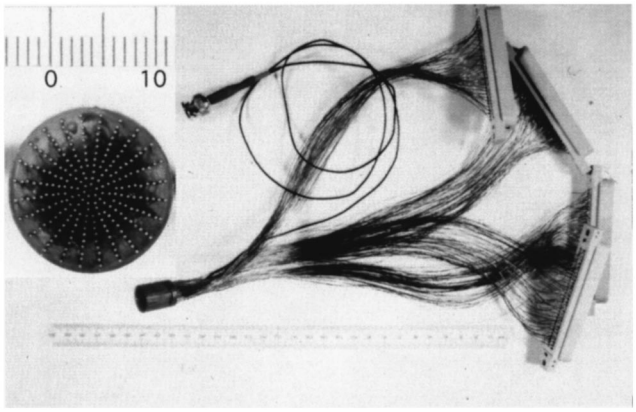

FIGURE 1. The electrode array. The upper left insert is the surface view of the electrodes with a scale in millimeters. The diameter of the electrode array is 16 mm, adequate to record the effects of strong cathodal stimulation, based upon previous observations of virtual cathodes on canine heart (see Ref. 20). The stimulation cathode is made of titanium wire and is located at the center of the assembly. There are 246 recording electrodes made of enameled copper wire. The wires of the electrodes are embedded in a cylinder of epoxy, except for the top 2 mm, which extrudes beyond the end of cylinder enabling the bath access to the tissue between the electrodes. The ends of the enameled copper wires are exposed and electroplated with silver, and then coated with silver chloride. The interelectrode radial spacing is 0.6 mm.

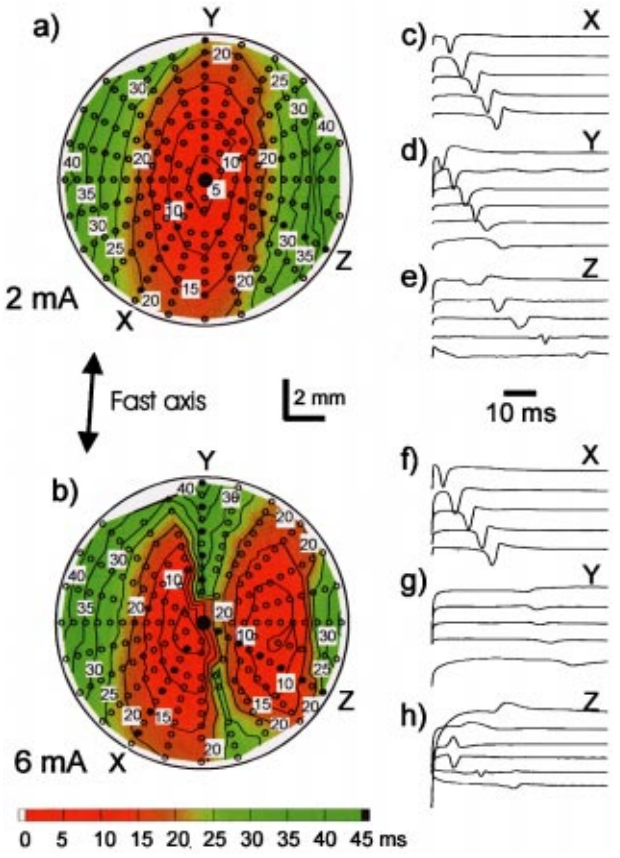

FIGURE 2. Activation triggered by 2 mA (a) and by 6 mA (b) cathodal stimuli in slice 1. The time of activation (indicated by colors, numbers, and isochrone lines) began at the end of the 0.33 ms stimuli. The large black dots at the centers of (a) and (b) indicate the sites of stimulation. The small circles (both open and filled) show the sites of each pair of bipolar recording electrodes. The traces of the bipolar signals from top to bottom in each group (c)–(h) correspond to the small filled circles from innermost to outermost along the corresponding directions *X–Z* in (a) and (b). The 2 mm bars indicate the spatial scale of the maps. The 10 ms time bar between (e) and (f) is the time scale for the traces. The color bar indicates the time of activation.

METHODS

Tissue Preparation

Epicardial slices of cardiac muscle (thickness: ~1 mm; surface area: between 4 and 20 cm^2) were cut with an electrodermatome (model B, Padgett Instruments, Kansas City, MO) from the left ventricles of canine hearts removed promptly after sacrifice. These epicardial slices have the properties of relatively uniform fiber orientation, anisotropic tissue resistivity, and a sufficient surface area, and have proven useful in many studies of cardiac activation.[1–5,7] The slices were placed immediately in an oxygenated solution (NaCl 128 mM, KCl 4.69 mM, $MgSO_4$ 1.18 mM, NaH_2PO_4 0.41 mM, $NaHCO_3$ 20.1 mM, $CaCl_2$ 2.23 mM, dextrose 11.1 mM, and HEPES 20 mM and bubbled with a gas mixture of 95% O_2 and 5% CO_2) having a pH within 7.35–7.40 and maintained at 37 °C by means of a circulating bath. After 1 h of healing, the slices were pinned to a Sylgard-coated platform in the bath. An electrode assembly (222 or 114 bipole pairs over 163 mm^2, depending on the pairing), as shown in Fig. 1, was placed in contact with the epicardial side of the slice. Continuous bubbling with 95% O_2 and 5% CO_2 kept the bath stirred and facilitated the access of superfusate to the epicardial surface through the space between the wire electrodes. The elliptically shaped isochrones following threshold stimuli [Figs. 2(a), 4(a), and 6(a)] indicated the healthiness and evenness of the tissue slices. A silver ground electrode with AgCl coating was placed in the bath.

Data Collection

Bipole recording electrodes with differential amplifiers were selected for the ease in recording local activation while reducing stimulation artifacts and for their compatibility with high data sampling rates. Both features were critical to the responses of tissue immediately following strong stimuli. Data were collected initially with a modular data acquisition system (MDAS) (model 7000, Kaye Instruments, Bedford, MA, 56 simultaneous-sample-and-hold analog-to-digital and two digital-to-analog channels), that was extended to 224 channels (four-fold multiplexing with switch boxes within 50 s),

and later with a 128-channel system comprised of two 64-channel data acquisition cards (AT-MIO64E, National Instruments, Austin, TX). An IBM–PC compatible computer running the data acquisition software LabVIEW™ (National Instruments) controlled either MDAS or the AT-MIO64E cards and processed data. A custom 128-channel differential amplifier connected the electrodes to one of the systems. The 246 electrodes in the assembly (Fig. 1) were paired radially either into 222 bipole pairs in four groups for the earlier system (neighboring bipoles went to different groups and shared the middle electrodes) or into 114 bipole pairs without electrode sharing for the later system. The consistency in isochrone lines as demonstrated in Figs. 2 and 4 indicated the validity of channel multiplexing used in the earlier system. MDAS or AT-MIO64E cards also drove two isolated current sources (Bloom Associates, Narberth, PA) to supply both the pacing (S1) and the test stimulation (S2) currents. The same experimental protocol and the same electrode assembly were used for both data acquisition systems.

Experimental Protocol

A cathodal stimulus (S2, between stimulation threshold and 30 mA, 0.33 ms) was delivered to the epicardium of each slice after ten cathodal pacing stimuli (S1, at twice the stimulation threshold, 0.33 ms) from the same platinum electrode located at the center of the electrode assembly. 1 s cycle length was used for both S1–S1 and S1–S2. Data were sampled at 3000 samples per second per channel for 100–700 ms starting from the onset of each S2 stimulus. For each epicardial slice, we started by determining the threshold of activation and then recorded the induced activations at incremental levels of S2 currents. We collected only the necessary data for constructing one activation map at each S2 level to minimize any unintended effects of strong S2.

Data Processing

Activation maps were formed either by combining data from 4 separate recordings at the same S2 strength collected within ~50 s with the earlier system (Figs. 2 and 4) or by using the data collected after a single S2 with the later system (Fig. 6). The time of activation at each bipole was determined at the peak activation in the corresponding electrogram. The recording sites in the maps represented the centers of each electrode bipole. We eliminated the sites with illegible activation that resulted from either poor electrode-tissue contact, or local in-excitable tissue (i.e., fat or blood vessels), or having a wave front perpendicular to the bipole, or where activation was masked by stimulation current (in the vicinity of the stimulation cathode). As most delayed activation and retrograde propagation occurred away from the site of stimulation in regions covered by multiple pairs of electrodes, a few missing recording sites did not affect our ability to identify retrograde propagation or delayed activation. The space between the recording sites was filled with data interpolation. The fast axis of threshold activation was determined from the map recorded with a threshold S2 [e.g., the 2 mA map in Fig. 2(a) and the 1 mA map in Fig. 4(a)]. Statistical data are expressed as mean ± standard deviation.

Since the polarity of the bipole electrode was proximal minus distal, outward propagation along each radial array of electrodes was identified when two or more neighboring traces of bipole signal had negative deflections and an earlier time of activation at the proximal bipole. Similarly, retrograde propagation (toward the site of stimulation) showed positive deflections in the signals and later activation at the proximal bipole. Both the outward and the retrograde propagations were the radial components of propagation wave fronts. The radial velocity was calculated by dividing the spatial separation of two neighboring bipoles, where activation propagated along the same radial direction, with their time differences in activation. Tangential velocity was not calculated since the circumferential electrode spacing increased with radius. Delayed activation was based on consistent visual observations of isochrone bending at the same location in two or more activation maps with consecutive levels of S2.

RESULTS

We observed elliptically shaped wave fronts of activation following S2s at or near the threshold of activation [e.g., Figs. 2(a), 4(a), and 6(a)] and two patterns of activation following strong S2s, as demonstrated in three typical cases (slices 1–3, Figs. 2–6) with the maps of activation propagation, as well as representative traces of extracellular bipolar recordings along selected radial directions (slices 1–2).

Slice 1

Following a 6 mA S2, a strip of activation delayed for about 20 ms in the general orientation of the fast axis of threshold activation (S2:2 mA) separated two transverse regions of early activation, one 4 mm away to the right of the cathode, and the other, 1 mm away to the left, started 5.3 and 3.7 ms after the S2, respectively [Fig. 2(b)]. Activation then propagated into surrounding tissue in all directions, including toward the cathode [Figs. 2(b), 2(h), and 3(c)], resulting in retrograde propagation transverse to the fast axis of threshold activation from the early activation site at right. Activation wave fronts collided along the strip of delayed activation. Radial conduction along the directions of *X*, *Y*, and *Z* represented

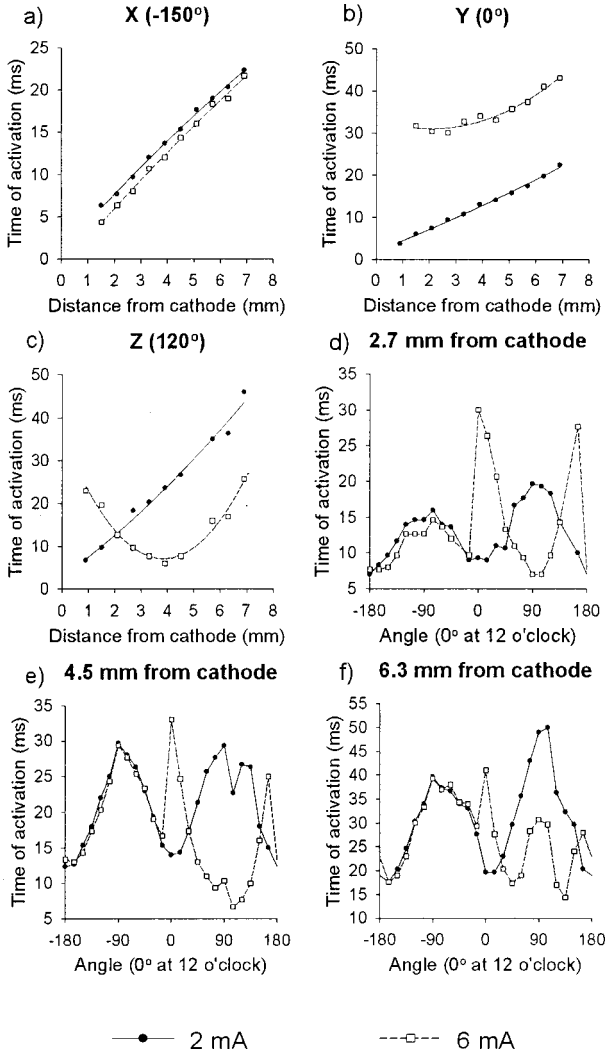

FIGURE 3. The time of activation along the radial directions *X*–*Z* (a)–(c) and on the rings 2.7, 4.5, and 6.3 mm from the cathode (d)–(f) corresponding to the maps in Fig. 2 (slice 1). The distances along *X*–*Z* in (a)–(c) are relative to the site of stimulation. The angles in (d)–(f) correspond to the maps with 0° at 12 o'clock and increase clockwise. The fast axis of threshold activation is around 0°/180°. The time starts at the end of the 0.33 ms stimuli.

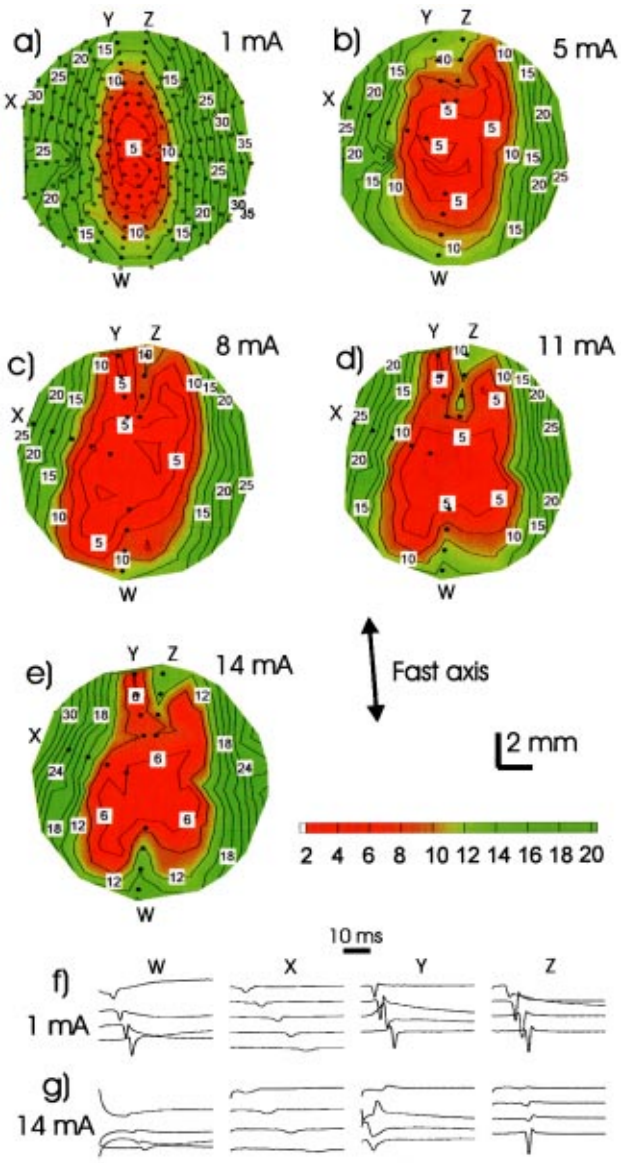

FIGURE 4. The activation propagation in slice 2. The small circles (both open and filled) show the sites of each pair of bipolar recording electrodes. The traces of bipolar signals from top to bottom in (f) and (g) correspond to the small filled circles from innermost to outermost along corresponding directions *W*–*Z* in (a) and (e). Similar to slice 1 (Fig. 2), central cathodal stimulation pulses with a duration of 0.33 ms and amplitudes as indicated in (a)–(e) were used to excite the tissue. The color bar indicates the time of activation relative to the end of the stimulus.

three typical types. Compared with the outward propagation following the 2 mA stimulus [Figs. 2(a), 2(c)–2(e)], activation along *X* following the 6 mA stimulus was slightly earlier with a similar velocity, significantly delayed along *Y*, and along *Z* the earliest activation occurred 4 mm away from the cathode and then propagated both inward to the cathode and outward to the edge of the recording area [Figs. 2(b), 2(f)–2(h), and 3(a)–3(c)]. The 6 mA S2 stimulus produced significant time delays along or near the fast axes of threshold activation (0° and 180°) relative to their neighboring directions on the 2.7 and 4.5 mm radius rings [Figs. 3(d)–3(e)].

Slice 2

Following S2s at ⩾8 mA, propagation delays (relative to neighboring directions) arose in two regions away from the cathode along the fast axis of threshold activation (*Z* and *W* in Figs. 4–5), and early activation occurred in a continuous region with the edge depressed at the fast axis of threshold activation [Figs. 4(d)–4(e)]. Retrograde propagation [along *Y* in Figs. 4(d)–4(e), and

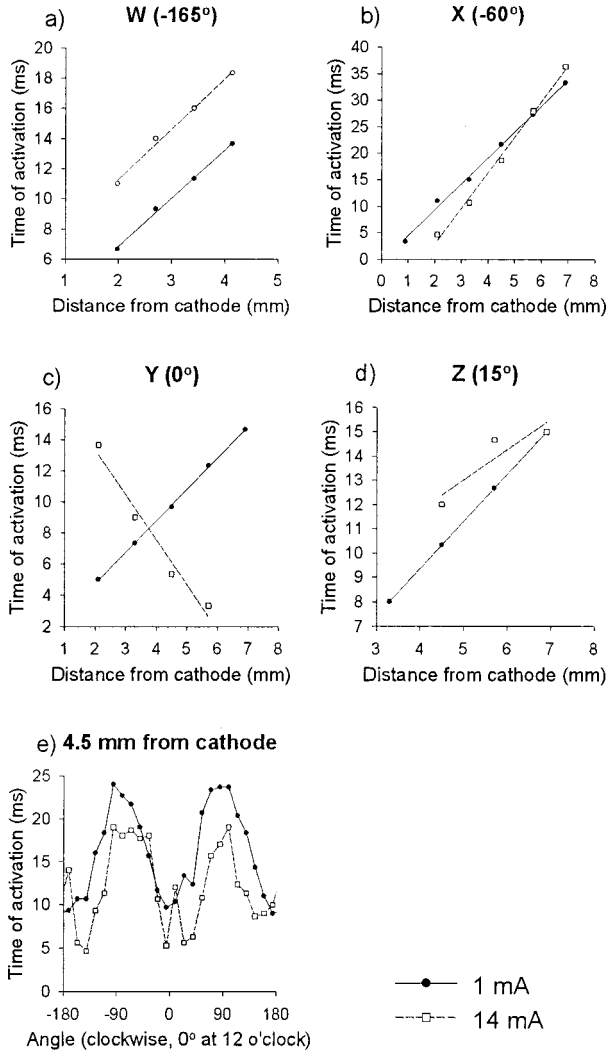

FIGURE 5. The time of activation along the radial directions *W–Z* (a)–(d), and on the ring 4.5 mm from the cathode (e) corresponding to the maps in Fig. 4 (slice 2). The distances along *W–Z* in (a)–(d) are relative to the site of stimulation. The angle in (e) corresponds to the maps with *Y* at 0° and increases clockwise. The fast axis of threshold activation is around 0°/180°. The time starts at the end of the 0.33 ms stimuli.

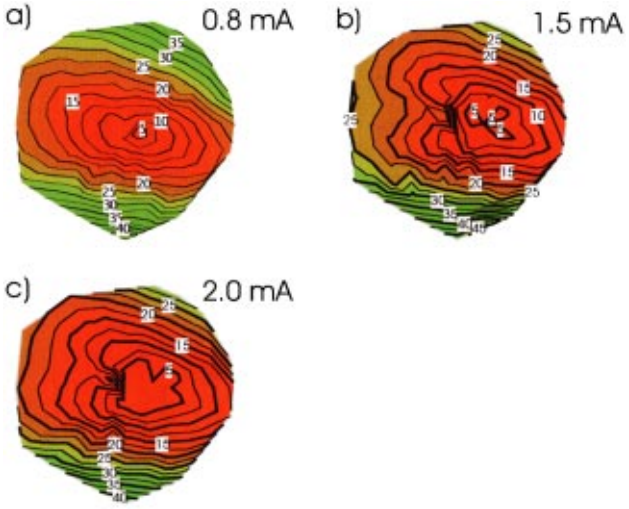

FIGURE 6. Activation propagation in slice 3. Each map is constructed from the data recorded with 114 pairs of bipole electrodes and the later data acquisition system following a single cathodal S2 stimulation at the center [duration: 0.33 ms, strength: 0.8 mA, (a); 1.5 mA, (b); and 2.0 mA, (c)]. The time of activation starts at the end of S2 stimulation.

5(c)] occurred next to the wedge of late activation (*Z*) following the 11 and the 14 mA stimuli. Along *X* (−60° from the fast axis of threshold activation), propagation was slower following the 14 mA stimulus (0.15 m/s) than following the 1 mA stimulus [0.20 m/s, Figs. 4(f)–4(g), and 5(b)]. On the ring 4.5 mm from the cathode [Fig. 5(e)], activation triggered by 1 mA stimulus had the earliest occurrences at −6° (at 9.7 ms) and at 174° (at 9.0 ms) and the latest occurrences at—96° (at 24 ms), at 84°, and at 99° (at 23.7 ms), as would be expected for elliptical isochrones induced by a low-current stimulus. With 14 mA stimulation, the time of activation was significantly delayed at the intersections of the fast axis of threshold activation and the 4.5 mm ring (6.7 ms delay near 0° and 8.3 ms delay near 180°, as compared to the neighboring sites on the ring). The delayed activation caused the notches in the isochrone lines at both sides of the stimulation electrode along the fast axis of threshold activation. The similar velocities along *W* for both 1 and 14 mA activations [Fig. 5(a)] demonstrate the stability of tissue excitability.

Slice 3

Delayed activation and subsequent wrap-around retrograde propagation along the fast axis of threshold activation occurred at a single side of the stimulation cathode following stimuli with strengths as low as less than twice the activation threshold (as shown with 1.5 and 2.0 mA stimuli in Fig. 6).

Combined Data From All Observations

The similarity of the data from different slices was readily evident when we displayed the data in polar plots [Figs. 7(a)–7(b)] according to the directions of the delayed activation and the retrograde propagation and the strength of stimuli normalized to their respective thresholds of activation, which differed among tissues. The polar angles indicated the direction of either delayed activation [Fig. 7(a)] or retrograde propagation [Fig. 7(b)] relative to the fast axes of threshold activation (the 0°–180° axes). We examined a total of 141 activation maps recorded on 42 slices from 14 hearts at stimulation

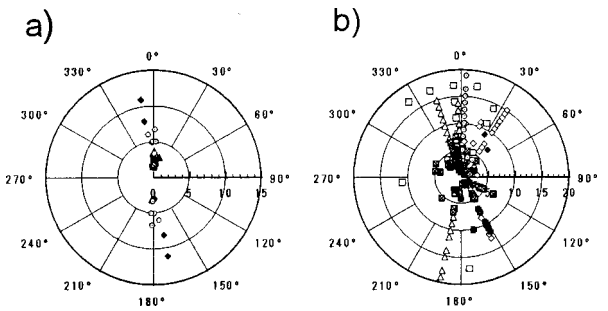

FIGURE 7. The directions (angles) of the delayed activation [0°±6°, *n*=32, (a)] and the retrograde propagation [2°±31°, *n*=179; velocity: 0.45±0.24 m/s, *n*=95; (b)] with the relative strengths of cathodal stimuli in multiples of the threshold for activation (radius). Each symbol represents data from one of the 13 slices [from 10 hearts, (a)] or from one of the 12 slices [from 8 hearts, (b)]. The fast axis of threshold activation is along 0°/180°. Separate cases were counted when retrograde propagations were observed following different S2s along the same direction, or along different directions following the same S2. Only one case of retrograde propagation was counted along a direction at the same S2 strength in the same slice.

strengths from the threshold of activation to more than 30 mA. Each activation map corresponded to one level of stimulation current in a tissue.

We observed delayed activation (relative to neighboring directions) with angular differences of $0°\pm6°$ ($n=32$) from the fast axis of threshold activation in 23 activation maps (9 on both sides and 14 on a single side of the cathode) recorded in 13 epicardial slices from 10 canine hearts [Figs. 7(a)]. Retrograde propagation occurred following cathodal stimuli (330 μs, 0.8–30 mA) along 179 radial lines in 85 activation maps out of a total of 141 maps in 12 slices from 8 hearts [Fig. 7(b)]. The average angular difference between the radial lines along which the retrograde propagations (velocity: 0.5 ± 0.2 m/s, $n=95$) occurred and the fast axis of threshold activation was $2°\pm31°$ ($n=179$). Therefore, retrograde propagation was not limited to the fast axis of threshold activation, but occurred over a wide dispersion of angles on either side of the axis. Stimulation strength did not affect the direction of retrograde propagation in the same tissue. This observation matched the predictions by bidomain models that stimulation strength should not affect the locations of virtual electrodes, only the degree of local depolarization or hyperpolarization. However, most retrograde propagation at transverse direction were observed at stimulation strengths of less than ten times of the threshold current [within the 10× ring in Fig. 7(b)], except one case. Significant stimulation artifacts near the stimulation electrode and the extended regions of instant activation reduced the cases of identifiable transverse retrograde propagation following strong stimuli (of >10× threshold). Therefore, most of our observations of retrograde propagation were within the 10× ring in Fig. 7(b). 5 of the above 12 slices showed retrograde propagation at stimulation strength of less than twice the threshold of activation.

DISCUSSION

Relation to Previous Studies

Bidomain simulations with uniform anisotropic resistivity (for either bulk tissue or tissue slices without a bath) predicted a transversely located dog-bone shaped region of instant depolarization (virtual cathode) separating two longitudinally located regions of instant hyperpolarization (virtual anodes) in the vicinity of the site of strong cathodal stimulation.[12,14] The relative sizes and locations of the virtual electrodes can be affected by the anisotropic tissue resistivity in both intracellular and extracellular spaces and by other details of cardiac muscle (such as the curvatures and the transmural rotation of fiber orientation). In the thin epicardial slices used in present study, the local microanatomy, the presence of a conductive bath, and the physical dimensions (thickness) also affected the distribution of the stimulation current and the electrophysiological responses. Therefore, the relative distances among virtual electrodes could have different combinations. While not predicted by the two-dimensional or bulk-tissue model studies[11,13–15] (without bath), the pattern of activation in Fig. 2(b) suggested that the pattern of activation propagation recorded with the bipolar electrode array could be different from the predicted pattern of virtual electrodes.[15] The regions of delayed activation could extend to the immediate vicinity of the stimulation cathode and divide the regions of early activation into two pieces. A similar filament of delayed depolarization along the fiber axis could also been seen in the frame 6 in Fig. 3(a) of a previous study[19] 6 ms after a 10 mA cathodal stimulus on the left ventricular epicardial surface of a rabbit heart. Our observations of delayed activations along the fast axis of threshold activation by strong stimuli were consistent with other measurements[19] supporting the predictions of virtual anodes by the bidomain simulations.

Retrograde propagation not only could occur along fiber axis as predicted by the simulations,[14] but could also occur transverse to the fast axis of threshold activation from the regions of early activation [Fig. 2(b)], resulting a wide dispersion in the direction of retrograde propagation (Fig. 7). Retrograde propagation along fiber axis by a point-injected cathodal stimulus was also observed *in vivo* in canine heart when Na^+ channel availability was reduced by high dosages of O-desmethyl encainide (ODE).[18] Therefore, both the point-injected cathodal current and high dosages of ODE are capable of

inducing retrograde propagation, an important condition for the initiation of the reentry of excitation and thus the fibrillation in cardiac muscle. We observed ~4 mm distances between the cathode and the early activation sites following strong cathodal stimuli (Figs. 2, 4, and 6), similar to the *in vivo* observations in canine hearts of $\sim 3 \pm 1$ mm[20] and of 3–4.5 mm.[18]

Figures 2(b) and 6(b)–6(c) agreed with the simulation prediction[14] that when virtual anodes created a sufficient delay in activation, the wave fronts of activation that originated from the two ends of the virtual cathode could collide outside the regions of virtual anodes. After the collision, activation in Figs. 6(b)–6(c) propagated both inward and outward. However, when the time delay in the regions of the expected virtual anodes was modest, as in Fig. 2(b), there was only delayed outward activation, instead of retrograde propagation.

Compared to the activation following the 1 mA stimulus, we observed a slower transverse velocity along *X* outside the region of early activation following the 14 mA stimulus in slice 2 [Figs. 4(f)–4(g), and 5(b)]. Such a slower velocity along *X* could be resulted from a change in the direction of local propagation or from a reduced local excitability by the instantaneous subthreshold depolarization at the transverse regions beyond the virtual cathode following a strong cathodal stimulus as demonstrated in bidomain simulations.[12,15]

In addition to the delayed activation and retrograde propagation, strong cathodal stimulation also produced cloverleaf-pattern net action currents in superfused canine epicardial slices, as computed from the magnetic field generated by net action currents recorded with a high-resolution superconducting quantum interference device magnetometer.[16]

New Observations

In this study we demonstrated a propagation pattern produced by cathodal stimulation with a strip of delayed activation along the general orientation of the fast axis of threshold activation separating two areas of early activation and the resulted retrograde propagation at right angles to the fast axis of threshold activation. This pattern is different from the expected dog-bone shaped region of early activation with retrograde propagation at or near the fast axis of threshold activation.[14] Furthermore, we showed that retrograde propagation could occur at a stimulation strength of less than twice the threshold of activation and that the strength of stimulus did not alter the direction of retrograde propagation. We concluded that cathodal stimulus could delay activation along the fast axis of threshold activation and induce retrograde propagation both along and transverse to the fast axis of threshold activation.

Limitations

Due to the spatial resolution of our electrode array, it was possible that an undetected thin filament of early activation passing underneath the site of stimulation connected the two regions of early activation in Fig. 2(b) forming a dog-bone shaped region of early activation, although such thin filament might not last long with the closely located neighboring regions of delayed activation. There could be differences between the orientation of muscle fibers and the fast axis of threshold activation. It was observed that the long axis of the elliptical wavefronts of activation rotated by more than 45° on the epicardial surface of a perfused left ventricle from guinea pig when the stimulation electrode moved inside ventricular wall from epicardium to endocardium, due to the transmural rotation of fiber orientation.[6] We limited the effects of transmural fiber rotation by using thin epicardial slices of ~1 mm thickness. However, the fiber orientation might still exhibit limited rotation within the slice thickness. The instantaneous activation triggered by strong stimuli could involve a thick layer of tissue with a larger variation in fiber orientation than would occur for threshold stimuli, resulting in angular shifts in the activation maps following different S2s. The computed radial velocity could be higher than the actual velocity when it contained nonradial components. Although symmetric maps were expected theoretically following a point stimulation in a perfect tissue formed by straight fibers, our recorded maps had certain unevenness [e.g., the strip of delayed activation followed a curved line passing by the site of stimulation in Fig. 2(b)]. We did not remove the unevenness in map symmetry so as to avoid possible artifacts introduced during data conversion. Strong stimuli could cause local electroporation at the site of stimulation.[17] We observed that both the delayed activation and the retrograde propagation occurred or initiated several mm away from the stimulation electrode. Thus, the possible electroporation in the immediate vicinity of the site of stimulation should not have significant effects on our observations. We only stimulated diastolic tissues to avoid the complexity of vulnerable period stimulation in tissue having a dispersion of refractoriness. Although sustained reentry was not observed due to diastolic stimulation and the limited size of the tissue sample, the retrograde propagation as demonstrated here is an important component of the mechanism of reentry.

Clinical Implications

This study suggested that point-injected cathodal current could induce retrograde propagation both along and transverse to the fast axis of threshold activation. Sustainable reentry could occur when retrograde propagation is combined with a slow velocity (e.g., by prema-

ture stimulation, or pathological or pharmacological responses). The possibility of inducing reentry might be decreased with changes in the shape of electrode or by using a better wave form of stimulation current different from the square pulses used in present study.

ACKNOWLEDGMENTS

The authors appreciate the generous assistance from Phillip E. Williams, Kareem Jabbour, Richard E. Parker, and Doss W. Neal. This research was supported in part by NIH Grant Nos. P01HL46681, R01HL58241, and HL52323, by Award No. 9930347Z from American Heart Association Midwest Affiliation, and by the Herman C. Krannert Fund, Indianapolis, IN.

REFERENCES

[1] Cabo, C., A. M. Pertsov, W. T. Baxter, J. M. Davidenko, R. A. Gray, and J. Jalife. Wave front curvature as a cause of slow conduction and block in isolated cardiac muscle. *Circ. Res.* 75:1014–1028, 1994.

[2] Davidenko, J. M., A. M. Pertsov, R. Salomonsz, W. Baxter, and J. Jalife. Spatiotemporal irregularities of spiral wave activity in isolated ventricular muscle. *J. Electrocardiol.* 24:Suppl: 113–122, 1992.

[3] Davidenko, J. M., A. M. Pertsov, R. Salomonsz, W. Baxter, and J. Jalife. Stationary and drifting spiral waves of excitation in isolated cardiac muscle. *Nature (London)* 355:349–351, 1992.

[4] Davidenko, J. M., P. F. Kent, D. R. Chialvo, D. C. Michaels, and J. Jalife. Sustained vortex-like waves in normal isolated ventricular muscle. *Proc. Natl. Acad. Sci. U.S.A.* 87:8785–8789, 1990.

[5] Delgado, C., B. Steinhaus, M. Delmar, D. R. Chialvo, and J. Jalife. Directional differences in excitability and margin of safety for propagation in sheep ventricular epicardial muscle. *Circ. Res.* 67:97–110, 1990.

[6] Efimov, I. R., B. Ermentrout, D. T. Huang, and G. Salama. Activation and repolarization patterns are governed by different structural characteristics of ventricular myocardium: experimental study with voltage-sensitive dyes and numerical simulations. *J. Cardiovasc. Electrophysiol.* 7:512–530, 1996.

[7] Gotoh, M., T. Uchida, W. J. Mandel, M. C. Fishbein, P. S. Chen, and H. S. Karagueuzian. Cellular graded responses and ventricular vulnerability to reentry by a premature stimulus in isolated canine ventricle. *Circulation* 95:2141–2154, 1997.

[8] Knisley, S. B. Transmembrane voltage changes during unipolar stimulation of rabbit ventricle. *Circ. Res.* 77:1229–1239, 1995.

[9] Knisley, S. B., B. C. Hill, and R. E. Ideker. Virtual electrode effects in myocardial fibers. *Biophys. J.* 66:719–728, 1994.

[10] Neunlist, M., and L. Tung. Spatial distribution of cardiac transmembrane potentials around an extracellular electrode: dependence on fiber orientation. *Biophys. J.* 68:2310–2322, 1995.

[11] Roth, B. J. Strength-interval curves for cardiac tissue predicted using the bidomain model. *J. Cardiovasc. Electrophysiol.* 7:722–737, 1996.

[12] Roth, B. J., and J. P. Wikswo, Jr. Electrical stimulation of cardiac tissue: a bidomain model with active membrane properties. *IEEE Trans. Biomed. Eng.* 41:232–240, 1994.

[13] Roth, B. J., and J. P. Wikswo, Jr. The effect of externally applied electrical fields on myocardial tissue. *Proc. IEEE* 84:379–391, 1996.

[14] Saypol, J. M., and B. J. Roth. A mechanism for anisotropic reentry in electrically active tissue. *J. Cardiovasc. Electrophysiol.* 3:558–566, 1992.

[15] Sepulveda, N. G., B. J. Roth, and J. P. Wikswo, Jr. Current injection into a two-dimensional anisotropic bidomain. *Biophys. J.* 55:987–999, 1989.

[16] Staton, D. J., R. N. Friedman, and J. P. Wikswo, Jr. High resolution SQUID imaging of octupolar currents in anisotropic cardiac tissue. *IEEE Trans. Appl. Supercond.* 3:1934–1938, 1993.

[17] Tung, L. Electroporation of cardiac cells. *Methods in Molecular Biology* 48:253–271, 1995.

[18] Turgeon, J., T. A. Wisialowski, W. Wong, W. A. Altemeier, J. P. Wikswo, Jr., and D. M. Roden. Suppression of longitudinal versus transverse conduction by sodium channel block. Effects of sodium bolus. *Circulation* 85:2221–2226, 1992.

[19] Wikswo, J. P., Jr., S.-F. Lin, and R. A. Abbas. Virtual electrodes in cardiac tissue: A common mechanism for anodal and cathodal stimulation. *Biophys. J.* 69:2195–2210, 1995.

[20] Wikswo, J. P. Jr., T. A. Wisialowski, W. A. Altemeier, J. R. Balser, H. A. Kopelman, and D. M. Roden. Virtual cathode effects during stimulation of cardiac muscle. Two-dimensional in vivo experiments. *Circ. Res.* 68:513–530, 1991.